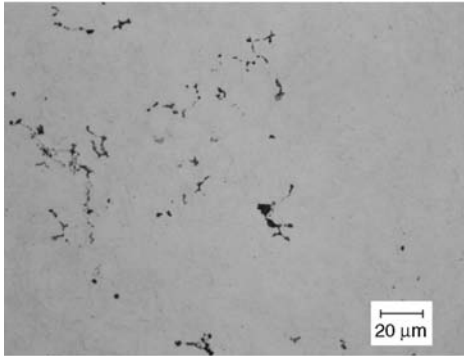


only 11 mass% Li is needed to form the body-centered cubic (bcc)  $\beta$  phase. When added to magnesium-aluminum alloys, equilibrium phases such as  $\text{AlLi}$ ,  $\text{Al}_2\text{Li}_3$ , and  $\text{Al}_4\text{Li}_9$  form.

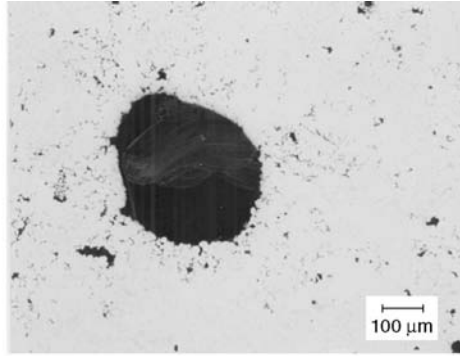
**Manganese.** In magnesium alloys that contain manganese but no aluminum, the manganese

appears as bluish-grey, primary elemental particles. Manganese combines with aluminum, when present, to form the compounds  $\text{AlMn}$ ,  $\text{Al}_4\text{Mn}$ , or  $\text{Al}_6\text{Mn}$ . These compounds may be contained in a single particle, with the ratio of aluminum to manganese increasing from the

center to the surface of the particle. Solution heat treatment transforms the particle to  $\text{Al}_6\text{Mn}$ . The presence of sufficient iron modifies the manganese-aluminum compounds to very hard manganese-aluminum-iron compounds.



(a)



(b)

**Fig. 19** As-polished surfaces of (a) AM60 and AZ91D pressure die cast specimens prepared using Masterprep alumina for the final step. Courtesy of G.F. Vander Voort, Buehler Ltd.

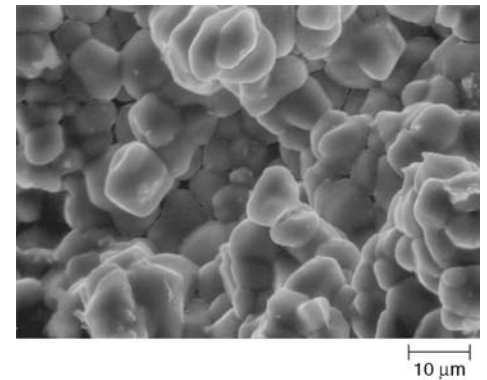


**Fig. 20** Scanning electron micrograph of the inter-dendritic microporosity associated with solidification defect shown in Fig. 2(b). Note the rounded appearance of the grains that solidified without proper metal feeding. Courtesy of B.R. Powell, General Motors Corporation

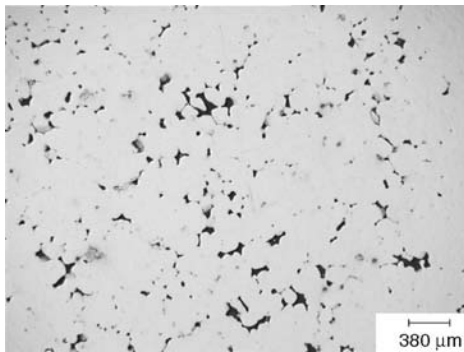
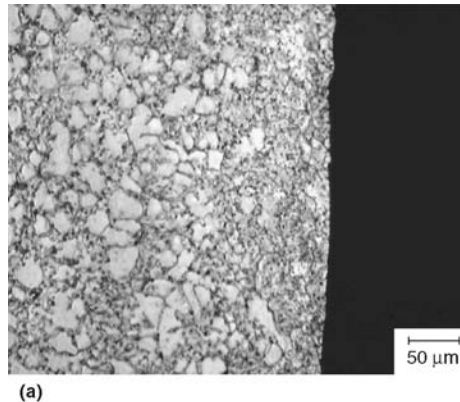
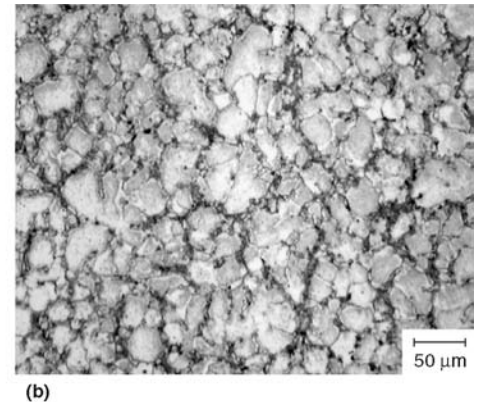


**Fig. 21** As-polished section of AZ31 direct chill cast billet showing solidification shrinkage. Courtesy of F. Pravidic, ARC Leichtmetallkompetenzzentrum Ranshofen

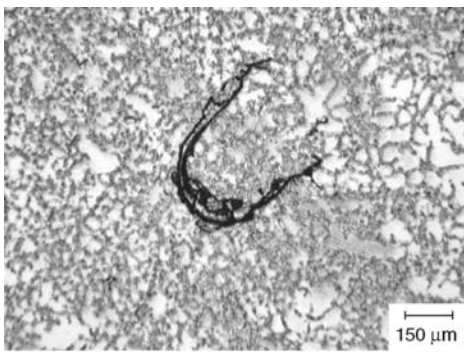


(a)

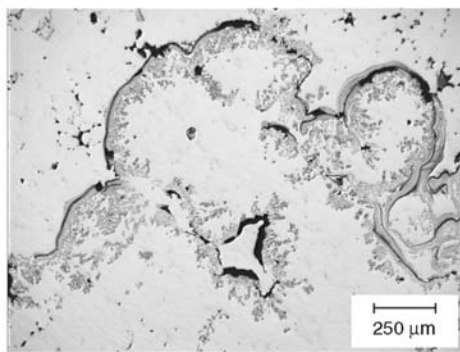


(b)

**Fig. 22** Microstructure of high-pressure die cast AM50A. (a) Near the surface. (b) Near the center of the section. The skin effect can be clearly seen in (a) where a high-integrity layer has formed, characterized by an extremely fine grain size and no porosity. (b) Due to a section thickness of  $\sim 4$  mm ( $\sim 0.16$  in.), the center section also cooled rapidly, resulting in a uniform distribution of fine grains. Etchant 5, Table 7. Courtesy of C.J. Padfield



(a)



(b)

**Fig. 23** (a) Example of an oxide film in an AM60B high-pressure die casting. Etchant 5, Table 7. Courtesy of C.J. Padfield. (b) An oxide cluster in a direct chill cast AZ31 billet. As-polished (unetched). Courtesy of F. Pravidic, ARC Leichtmetallkompetenzzentrum Ranshofen

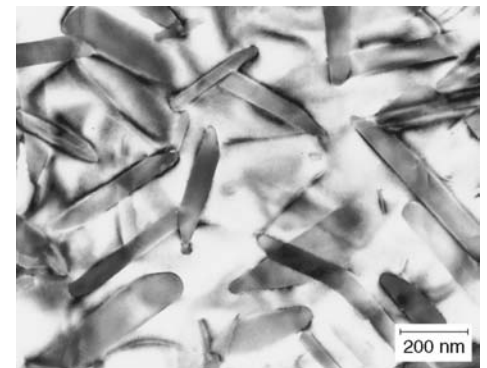


**Fig. 24** Transmission electron micrograph of AZ91 showing continuous (Widmanstätten) precipitation of  $\text{Al}_{12}\text{Mg}_{17}$  after 8 h at  $200^\circ\text{C}$  ( $390^\circ\text{F}$ ). Courtesy of J.-F. Nie, Monash University

Particles of manganese-aluminum compound often occur in the form of chunks and needles. The particles sometimes have irregular, sawtooth surfaces, which result from growth in the mushy and the early solid stages.

**Rare Earth Metals.** Because of the low solubility of rare earth metals in magnesium, there is usually an excess of  $Mg_9RE$  compound at the grain boundaries of magnesium-mischmetal and magnesium-didymium alloys. In Mg-Y-Nd alloys, the precipitation sequence ends with the equilibrium  $\beta$  phase, which has a composition of  $Mg_{14}Nd_2Y$  (Ref 70). Figure 26 is an electron micrograph showing the precipitate structure after 48 h aging at 250 °C. In Mg-Ag-RE alloys, the equilibrium phase is  $Mg_{12}Nd_2Ag$ .

When added to magnesium-aluminum alloys, a lamellar interdendritic phase forms with the composition  $Al_{11}RE_3$  ( $\sim Al_4RE$ ). A minor particulate interdendritic phase also forms with the composition  $Al_2RE$  (Ref 45). The microstructure of AE42 is described in Fig. 27.

**Silicon** is present in magnesium alloys as particles of  $Mg_2Si$ . These particles are distinguished by their angular outline, smooth edges, and light-blue color.

**Silver.** Silver contributes to precipitation hardening by forming incoherent precipitates with the composition  $Mg_{12}Nd_2Ag$ . These precipitates contribute to increased strength and creep resistance.

**Strontium.** Alloying with strontium results in different microstructures depending on the strontium-to-aluminum ratio. For strontium-to-aluminum ratio  $\sim 0.3$ ,  $Al_3Sr$  is the only intermetallic phase present (Fig. 28). The strontium-to-aluminum ratio controls the formation of  $Al_{12}Mg_{17}$ —at very low ratios there is insufficient strontium to tie up all of the available aluminum,

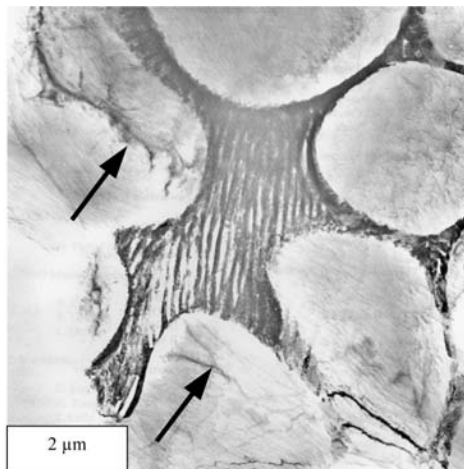


**Fig. 25** Brightfield transmission electron micrograph of AXJ530. The microstructure consists of primary magnesium with aluminum in solid solution surrounded by a grain-boundary eutectic phase. The eutectic phase has a lamellar structure consisting of alternating layers of magnesium and the intermetallic  $(Al,Mg)_2Ca$ . Note the dislocation networks within the primary magnesium grains (arrows). Courtesy of B.R. Powell, General Motors Corporation

and  $Al_{12}Mg_{17}$  can form (Ref 10). At higher ratios, a ternary phase Mg-Al-Sr phase is also observed (Fig. 29). Figure 30 shows the lamellar structure of the eutectic phase.

**Thorium.** At the eutectic temperature of 589 °C (1092 °F), 4.5% Th is soluble in magnesium; however, because of alloy segregation, magnesium alloys containing as little as 2% Th often contain a divorced eutectic and show massive magnesium-thorium compound at the grain boundaries. At temperatures below the eutectic, this compound is also precipitated from solid solution. In castings, the precipitate forms within grains and is seldom visible. In worked struc-

tures, the precipitate is often clearly visible at grain boundaries.

The addition of thorium to magnesium-zinc alloys changes the degenerate eutectic, which contains magnesium-zinc compound, to a lamellar eutectic, which contains a Mg-Th-Zn compound.

**Tin** is useful when alloyed with magnesium in combination with small amounts of aluminum. It substitutes in several intermetallic phases including  $Al_9(Ca,Sn)$  and  $Al_2(Ca,Sn,Sr)$ .

**Zinc.** At the eutectic temperature of 340 °C (644 °F), 6.2% Zn is soluble in magnesium, but at lower temperatures there is general precipita-

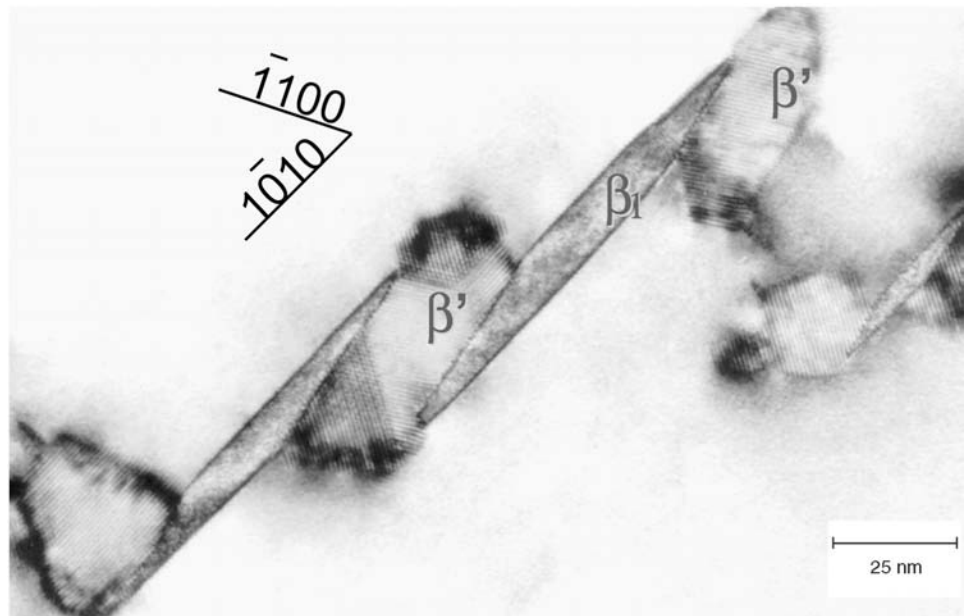


**Fig. 26** Brightfield electron micrograph of sand cast WE54 after aging for 48 h at 250 °C (480 °F). The image shows assemblies of plate-shaped and irregular globular precipitates. With extended aging, the  $\beta'$  phase decomposes, and the  $\beta_1$  plates transform in situ to the equilibrium phase, although the peak-aged microstructure contains all three phases. Courtesy of J.-F. Nie, Monash University

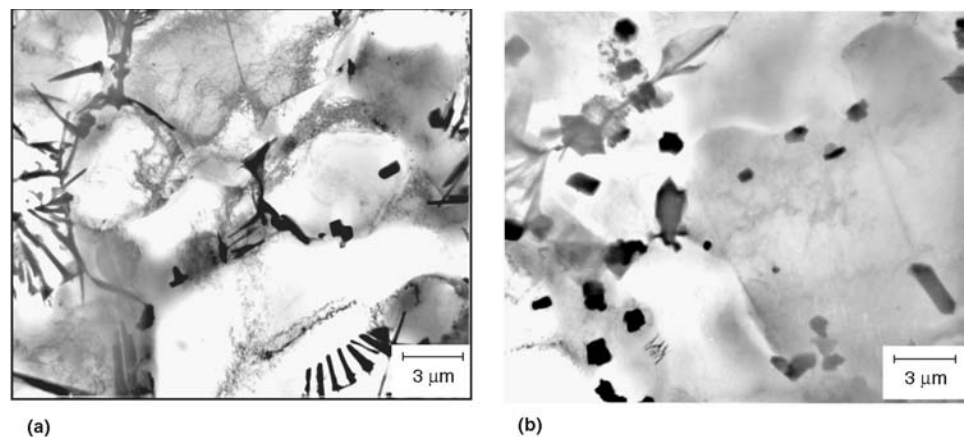


**Fig. 27** Brightfield transmission electron micrograph of high-pressure die cast AE42. (a) Primary magnesium with aluminum in solid solution surrounded by the lamellar phase  $Al_{11}RE_3$  and the particulate phase  $Al_2RE$ . (b) After exposure to temperature above 175 °C (345 °F), the presence of the lamellar phase is reduced and the particulate phase dominates. This may help to explain the loss in creep resistance of this alloy at these temperatures. B.R. Powell, General Motors Corporation

tion of magnesium-zinc compound whose particles are not clearly resolvable by optical or electron microscopy until the alloy is overaged (see Fig. 31 and 32).

When zinc is added to magnesium-aluminum alloys, the magnesium-aluminum eutectic takes a completely divorced form, in which massive particles of  $\text{Al}_{12}\text{Mg}_{17}$  compound—or of  $(\text{Al,Zn})_{49}\text{Mg}_{32}$  compound, if the ratio of zinc to aluminum exceeds 1 to 3—are surrounded by magnesium solid solution. Additions of zinc to magnesium/rare-earth metal alloys increase the amount and continuity of the compound at the grain boundaries. Zinc additions also promote the change of the magnesium/rare-earth eutectic to the divorced form. By adding approximately

2% Zn to magnesium alloys containing at least 2% Th, an acicular, or platelet, form of compound develops. The acicular form entirely replaces the massive form when the zinc content is increased to approximately 3%, but it again disappears when the zinc content is further increased to above 5%.

**Zirconium**, in amounts less than 1%, is alloyed with magnesium and added to magnesium alloys containing zinc, rare earth metals, or thorium. The remarkable effectiveness of zirconium in grain-refining magnesium has been explained by the similarities in crystal structure and lattice parameters of the two elements. The lattice parameters of zirconium ( $a = 0.323 \text{ nm}$ ,  $c = 0.514 \text{ nm}$ ) are very similar to those of magne-

sium ( $a = 0.320 \text{ nm}$ ,  $c = 0.520 \text{ nm}$ ). Magnesium grains nucleate epitaxially on the (0001) basal planes of hcp  $\alpha$ -zirconium phase crystals, which are first to separate during cooling.

In binary magnesium-zirconium alloys, zirconium-rich particles can be seen within grains and near grain boundaries. Zirconium-rich cores generally appear as either elliptical or nearly circular form on polished sections. Electron microscopy using backscatter detection shows the particles to be bright points within a highly cored primary magnesium grain (Ref 71). In the more complex alloys, zirconium may form compounds with zinc and with certain elements that are impurities in those alloys, such as aluminum, iron, silicon, and hydrogen.

#### ACKNOWLEDGMENT

The author would like to thank the following individuals for contributing images to this article: Éric Baril of Noranda, Jian-Feng Nie of Monash University, Cory Padfield of Hyundai America, Bob Powell of GM, Franka Pravidc of ARC Leichtmetallkompetenzzentrum Ranshofen, Elke Schaberger of Gießerei-Institut, RWTH Aachen, and George Vander Voort of Buehler Ltd. Also, the author is extremely grateful for the thorough review and helpful discussions provided by Cory Padfield during this project.

#### REFERENCES

1. L. Gaines et al., *Analysis of the Potential for New Automotive Uses of Wrought Magnesium*, Center for Transportation Research National Laboratory, United States Department of Energy, 1996 (available to the public from National Technical Information Service, U.S. Department of Commerce)

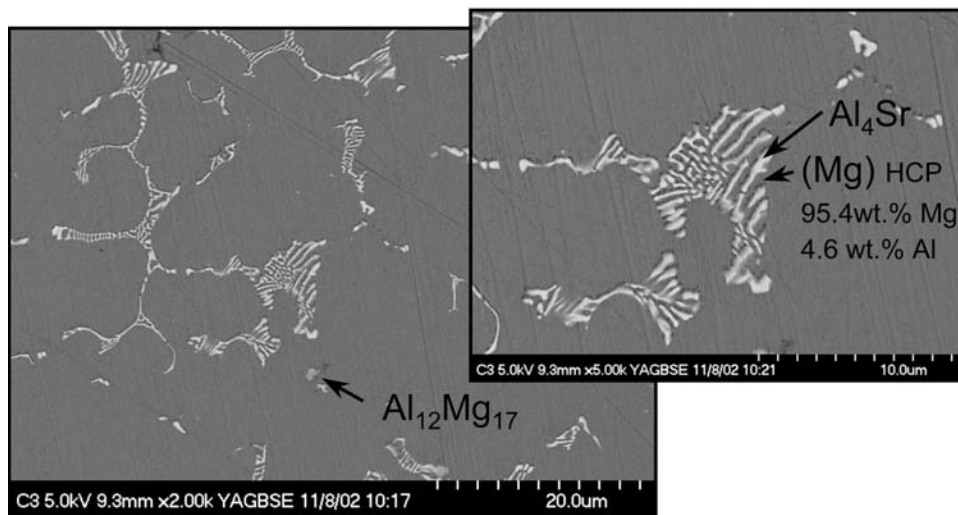


**Fig. 28** Backscattered electron micrograph (FEG-SEM) of high-pressure die cast AJ62L (low strontium). Microstructure consists of primary magnesium grains surrounded by grain-boundary eutectic phase.  $\text{Al}_4\text{Sr}$  is the main intermetallic phase present, but due to the low strontium content, some  $\text{Al}_{12}\text{Mg}_{17}$  also forms. Courtesy of Éric Baril, Noranda

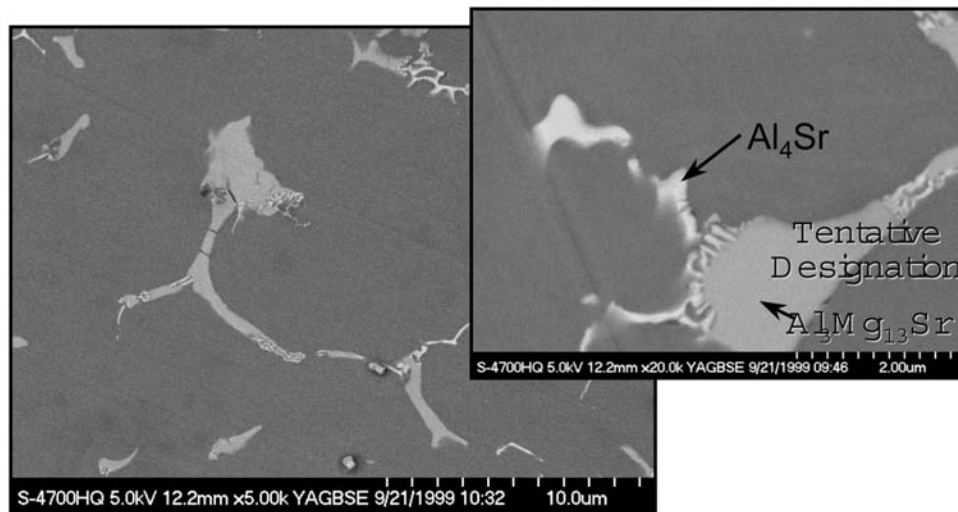


**Fig. 29** Backscattered electron micrograph (FEG-SEM) of high-pressure die cast AJ52. Microstructure consists of primary magnesium grains surrounded by grain-boundary eutectic phase. Two intermetallic phases are present:  $\text{Al}_4\text{Sr}$  and a ternary  $\text{Al-Mg-Sr}$  phase. Courtesy of Éric Baril, Noranda

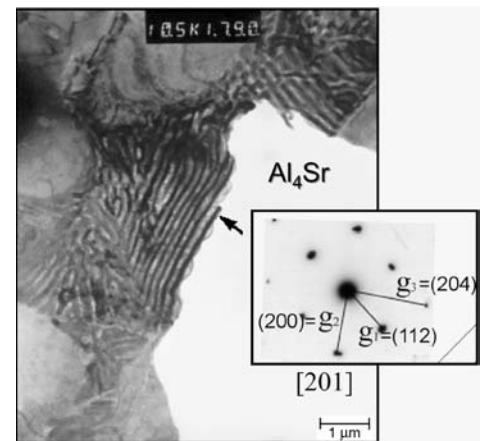


**Fig. 30** Transmission electron micrograph and diffraction pattern of high-pressure die cast AJ52. The eutectic phase has a lamellar structure consisting of alternating layers of magnesium and  $\text{Al}_4\text{Sr}$ . The lamellar structure is similar to that of AE42 and AXJ530. Courtesy of Éric Baril, Noranda

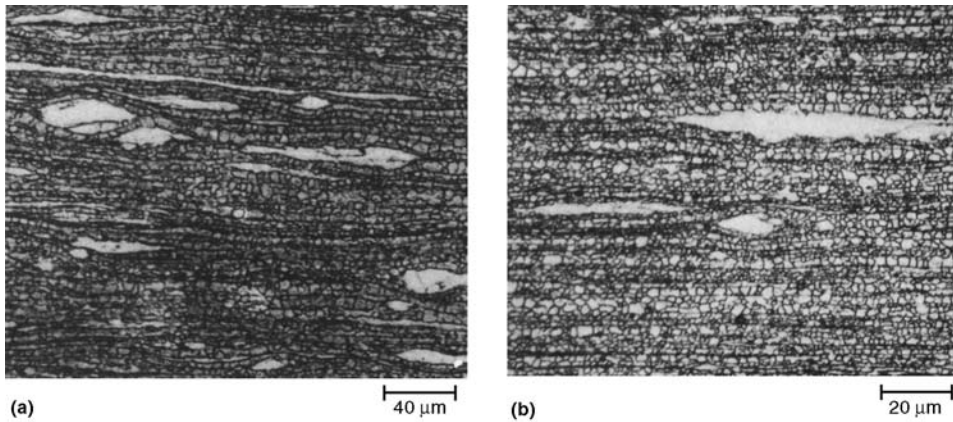


**Fig. 31** ZK60A-F extrusion. (a) Longitudinal view of banded hot-worked structure. Small, recrystallized grains. Light islands are solid-solution deficient in zinc and zirconium (due to alloy segregation) and so more resistant to hot working. Etchant 6, then etchant 4 (Table 7). 250 $\times$ . (b) Artificially aged to the T5 temper. Despite the higher magnification, structure appears the same as in (a) (precipitate formed during aging is irresolvable by microscopy). Etchant 7 for 7 s, then etchant 6, 1 s (Table 7). 500 $\times$

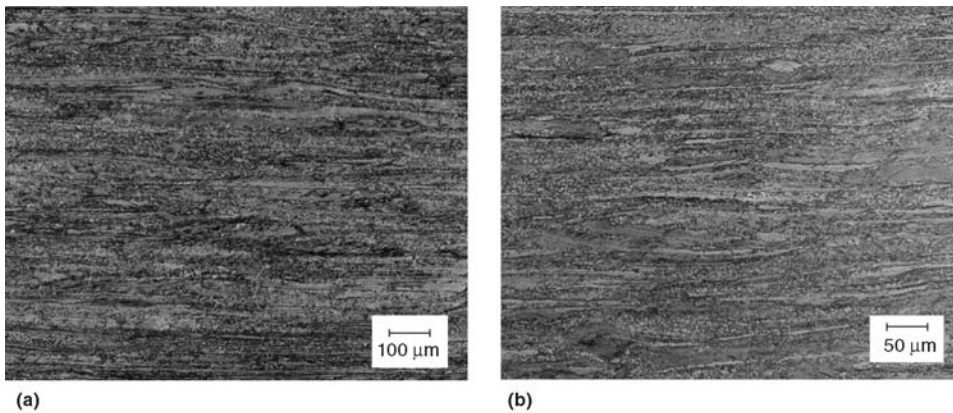


**Fig. 32** Two views of the microstructure of wrought Mg-2.8%Zn-0.62%Zr etched with acetic-picral and viewed with polarized light plus a sensitive tint filter. Etching clearly depicts the deformation anisotropy, as well as alloy segregation leading to grain size variation. The grain structure is not recrystallized after working. Courtesy of G.F. Vander Voort, Buehler Ltd.

2. "Practice for Codification of Certain Nonferrous Metals and Alloys, Cast and Wrought," B 275, *Annual Book of ASTM Standards*, ASTM International
3. "Practice for Temper Designation of Magnesium Alloys, Cast and Wrought," B 296, *Annual Book of ASTM Standards*, ASTM International
4. "Standard Practice for Numbering Metals and Alloy (UNS)," E 527, *Annual Book of ASTM Standards*, ASTM International
5. "Magnesium and Magnesium Alloys—Magnesium and Magnesium Alloy Anodes, Ingots and Castings—Designation System," EN 1754, European Committee for Standardization
6. "Magnesium and Magnesium Alloys—Magnesium Alloy Ingots and Castings," ISO 16220, International Organization for Standardization
7. "Magnesium and Magnesium Alloys—Magnesium Alloy—Wrought Magnesium

- Alloys," ISO 3116, International Organization for Standardization
8. D. Webb, "Magnesium Supply and Demand," Proc. 60th Annual World Magnesium Conference, International Magnesium Association, 2003
9. D. Kramer, Magnesium, *Minerals Yearbook*, Vol I, Metals and Minerals, U.S. Government Printing Office, 2002
10. M.O. Pekguleryuz et al., Creep Resistant Magnesium Alloys for Powertrain Applications, *Adv. Eng. Mater.*, Vol 5 (No. 12), 2003, p 866–878
11. B.R. Powell et al., "Progress Toward a Magnesium-Intensive Engine: The USAMP Magnesium Powertrain Cast Components Project," Technical Paper Series 2004-01-0654, SAE International
12. M.O. Pekguleryuz et al., "Magnesium-Based Casting Alloys Having Improved Elevated Temperature Performance," United States Patent 6,322,644

13. M.O. Pekguleryuz et al., Development of Creep Resistant Mg-Al-Sr Alloys, *Magnesium Technology 2001*, TMS (The Minerals, Metals, & Materials Society) 2001, p 119–125
14. B.R. Powell et al., "Creep-Resistant Magnesium Alloy Die Castings," United States Patent 6,264,763
15. B.R. Powell et al., Creep and Microstructure of Magnesium-Aluminum-Calcium Based Alloys, *Metall. Mater. Trans. A*, Vol 33A, March 2002, p 567–574
16. T. Baba et al., "Heat-Resistant Magnesium Alloy," United States Patent 5,811,058
17. S. Koike et al., "Development of Lightweight Oil Pans Made of a Heat-Resistant Magnesium Alloy for Hybrid Engines," Technical Paper Series 2000-01-1117, SAE International
18. B. Bronfin et al., "Magnesium Alloy for High Temperature Applications," United States Patent 6,139,651
19. B. Bronfin et al., Development of New Magnesium Alloys for Advanced Applications, *Magnesium—Alloys and Technologies*, Wiley-VCH, 2003
20. P. Bakke et al., "Die Cast Magnesium Alloys for High Temperature Applications," Technical Paper Series 2003-01-0189, SAE International
21. B. Bronfin et al., "High Strength Creep Resistant Magnesium Alloys," United States Patent Application US 2003/0084968 A1
22. B. Bronfin et al., "High Temperature Mg Alloys for Sand and Permanent Mold Casting Applications," Technical Paper Series 2004-01-0656, SAE International
23. C.J. Bettles et al., "Creep Resistant Magnesium Alloy," International Publication Number WO 2004/001087 A1, World Intellectual Property Organization
24. C.J. Bettles et al., "AMC-SC1: A New Mg Alloy Suitable for Powertrain Applications," Technical Paper Series 2003-01-1365, SAE International
25. G.F. Vander Voort, Metallography of Magnesium and its Alloys, *Tech-Notes*, Vol 4 (No. 2), Buehler Ltd., 2004
26. Light Metals, *Buehler SUM-MET—The Science Behind Materials Preparation*, Buehler Ltd., 2004
27. K.J. Clark, Magnesium Alloys, *Metallography and Microstructures*, Vol 9, *ASM Handbook*, American Society for Metals, 1985, p 425–434
28. J.M. Tartaglia et al., Magnesium Alloy Ingots: Chemical and Metallographic Analyses, *JOM*, Nov 2001, p 16–19
29. E. Schaberger et al., Development of a Metallographic Microstructure Characterization for the High-Purity Magnesium Alloy, *Pract. Metallogr.*, Vol 35 (No. 6), 1998, p 306–315
30. Metalog Method 350, *e-Metalog*, Struers A/S, Rødovre, Denmark
31. E. Schaberger et al., The Development of an Electrolytic Etching Process for Examining

- the Microstructure of Thixocast Magnesium Alloy AZ91 hp, *Pract. Metallogr.*, Vol 37 (No. 3), 2000, p 140–149
32. Metalog Method A, *Struers Metalog Guide*, Struers A/S, Rødovre, Denmark, 2000
  33. L.-Y. Wei et al., Characterisation of Manganese Containing Intermetallic Particles and Corrosion Behaviour of Die Cast Mg-Al Based Alloys, *Magnesium Technology 2000*, TMS (The Minerals, Metals, & Materials Society), 2000, p 153–160
  34. T. Mitchell et al., Microstructure Property Studies of In Situ Worked PVD Mg-Ti Alloys, *Magnesium Technology 2000*, TMS (The Minerals, Metals, & Materials Society), 2000, p 169–174
  35. M. Cabibbo et al., Microstructural Study and Mechanical Properties of Thixoformed AZ91, *Magnesium Technology 2000*, TMS (The Minerals, Metals, & Materials Society), 2000, p 301–307
  36. E.A. Nyberg et al., Microstructure and Microchemistry of Creep Resistant Magnesium Alloys, *Magnesium Technology 2001*, TMS (The Minerals, Metals, & Materials Society), 2001, p 169–1173
  37. L. Shepeleva et al., TEM Study of the As-Cast and Aged Microstructures of Mg-Al-Zn Alloys and the Influence of Zn Content on Precipitation, *Magnesium Technology 2001*, TMS (The Minerals, Metals, & Materials Society), 2001, p 189–194
  38. M. Cabibbo et al., Microstructural Study After Solution Treatments of a Thixocast AZ91, *Magnesium Technology 2001*, TMS (The Minerals, Metals, & Materials Society), 2001, p 211–216
  39. T. Horie et al., Development of High Creep-Resistant Magnesium Alloy Strengthened by Ca Addition, *Magnesium Technology 2000*, TMS (The Minerals, Metals, & Materials Society), 2000, p 261–269
  40. R.V. Allen et al., Magnesium Alloy Sheet Produced by Twin-Roll Casting, *Magnesium Technology 2001*, TMS (The Minerals, Metals, & Materials Society), 2001, p 75–79
  41. I.P. Moreno et al., Microstructure and Creep Behavior of a Die Cast Magnesium Rare Earth Alloy, *Magnesium Technology 2002*, TMS (The Minerals, Metals, & Materials Society), 2002, p 111–116
  42. G. S. Song et al., Enhancement of the Properties of Mg-Li Alloys by Small Alloying Additions, *Magnesium Technology 2003*, TMS (The Minerals, Metals, & Materials Society), 2003, p 77–79
  43. C. Mendis et al., Effects of Ca Additions on Microstructures, Age Hardening Response and Creep Behavior of Mg-8Zn-4Al Casting Alloy, *Magnesium Technology 2003*, TMS (The Minerals, Metals, & Materials Society), 2003, p 183–188
  44. F. Czerwinski et al., Correlating the Microstructure and Tensile Properties of a Thixomolded AZ91D Alloy, *Acta Mater.*, Vol 49, 2001, p 1225–1235
  45. B.R. Powell et al., The Relationship Between Microstructure and Creep Behavior in AE42 Magnesium Die Casting Alloy, *Magnesium Technology 2001*, TMS (The Minerals, Metals, & Materials Society), 2001, p 175–181
  46. M.T. Rowley, Ed., *International Atlas of Casting Defects*, American Foundry Society, 1993
  47. Testing and Inspection of Casting Defects, *Casting*, Vol 15, *ASM Handbook*, ASM International, 1988, p 544–561
  48. W.G. Walkington, *Die Casting Defects—Causes and Solutions*, North American Die Casting Association, 1997
  49. *Castings, Classification and Inspection of MIL-STD-2175*, Department of Defense Single Stock Point for Military Specifications and Standards, Document Automation and Production Service
  50. B.R. Powell et al., The Die Castability of Calcium-Containing Magnesium Alloys: Thin-Wall Computer Case, *Magnesium Technology 2002*, TMS (The Minerals, Metals, & Materials Society), 2002, p 123–129
  51. C.R. Dallam et al., Characterization of Welds, *Welding, Brazing, and Soldering*, Vol 6, *ASM Handbook*, ASM International, 1993, p 97–106
  52. Overview of Weld Discontinuities, *Welding, Brazing, and Soldering*, Vol 6, *ASM Handbook*, ASM International, 1993, p 1073–1080
  53. *Guide for the Visual Examination of Welds*, AWS B1.11,
  54. “Welding and Allied Processes—Classification of Geometric Imperfections in Metallic Materials—Part 1: Fusion Welding,” ISO 6520-1, International Organization for Standardization
  55. “Welding and Allied Processes—Classification of Geometric Imperfections in Metallic Materials—Part 2: Welding with Pressure,” ISO 6520-2, International Organization for Standardization
  56. *SAE Magnesium Alloys AMS Handbook*, AHB-002, SAE International, 1997
  57. P. Chaudhury et al., Forging of Magnesium Alloys, *Forming and Forging*, Vol 14, *ASM Handbook*, ASM International, 1988
  58. G. Dieter, Workability Tests, *Forming and Forging*, Vol 14, *ASM Handbook*, ASM International, 1988
  59. J.C. Grebets et al., Measuring the Cleanliness of Recycled Magnesium for Automotive Applications: A Detailed Examination of the Fracture Brightness Technique, *Light Metal Age*, Aug 1997, p 60–69
  60. D. Argo et al., Chemical Composition and Cleanliness During Recycling of the AJ52 Magnesium Strontium Alloy, *Magnesium Technology 2003*, TMS (The Minerals, Metals, & Materials Society), 2002, p 33–37
  61. “Standard Test Method for Macroetching Metals and Alloys,” E 340, *Annual Book of ASTM Standards*, ASTM International
  62. I.J. Polmear, *Metallurgy of the Light Metals*, Halstead Press (John Wiley & Sons, Ltd.), 1996
  63. S. Housh et al., Selection and Application of Magnesium and Magnesium Alloys, *Properties and Selection: Nonferrous Alloys and Special-Purpose Materials*, Vol 2, *ASM Handbook*, ASM International, 1990
  64. Properties of Magnesium Alloys, *Properties and Selection: Nonferrous Alloys and Special-Purpose Materials*, Vol 2, *ASM Handbook*, ASM International, 1990
  65. C.S. Roberts, *Magnesium and Its Alloys*, John Wiley and Sons, 1960
  66. E.F. Emley, *Principles of Magnesium Technology*, Pergamon Press Ltd., 1966
  67. G.V. Raynor, *The Physical Metallurgy of Magnesium and Its Alloys*, Pergamon Press, 1959
  68. A. Beck, *The Technology of Magnesium and Its Alloys*, F.A. Hughes and Co., Ltd., 1943
  69. B.E. Carlson, “Influence of Processing Variables and Aluminum Content on the Microstructure and Mechanical Properties of Cast Mg-Al Alloy,” Ph.D. dissertation, University of Michigan—Ann Arbor, 1997
  70. J.-F. Nie et al., Characterisation of Strengthening Precipitate Phases in a Mg-Y-Nd Alloy, *Acta Mater.*, Vol 48, 2000, p 1691–1703
  71. M. Qian et al., Characteristic Zirconium-Rich Coring Structures in Mg-Zr Alloys, *Scr. Mater.*, Vol 46, 2002, p 649–654

## SELECTED REFERENCES

- J.R. Davis, *Alloying: Understanding the Basics*, ASM International, 2001
- D.A. Kramer, Magnesium and Magnesium Alloys, *Kirk-Othmer Encyclopedia of Chemical Technology*, 4th ed., John Wiley & Sons, 2001
- V. Kree et al., The Metallographical Examination of Magnesium Alloys, *Pract. Metallogr.*, Vol 41 (No. 5), 2004
- “Microstructure of Magnesium Based Die-casting Alloys,” *Hydro Magnesium Diecaster Bulletin* No. 3, 1999
- “Standard Guide for Preparation of Metallographic Specimens,” E 3, *Annual Book of ASTM Standards*, ASTM International
- “Standard Practice for Microetching Metals and Alloys,” E 407, *Annual Book of ASTM Standards*, ASTM International

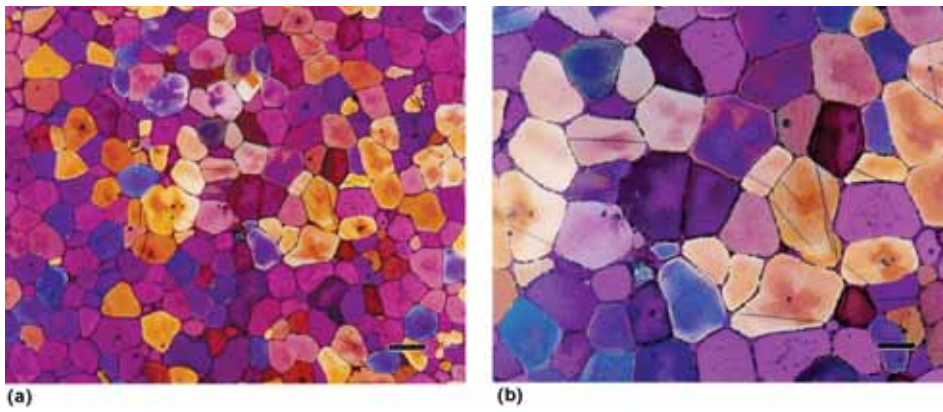


**Fig. 54** Microstructure of as-cast Mg-2.5% rare earth elements-2.11%Zn-0.64%Zr revealed using the acetic-picral etch and viewed with polarized light illumination plus a sensitive tint filter. Alloy segregation (coring) and grain boundaries are well depicted in these images, as are the mechanical twins present. (G.F. Vander Voort, Buehler Ltd.)

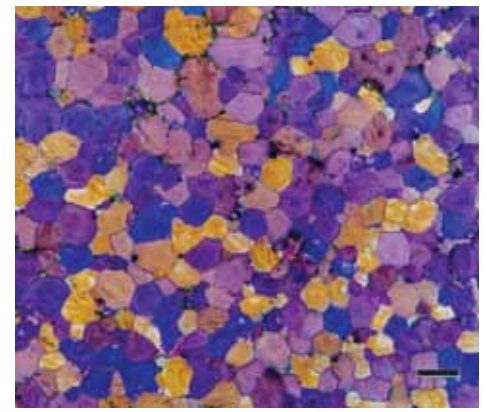


**Fig. 55** Microstructure of as-cast Mg-4.6%Zn-0.76%Zr revealed using acetic-picral etch and viewed with polarized light illumination plus a sensitive tint filter. (G.F. Vander Voort, Buehler Ltd.)

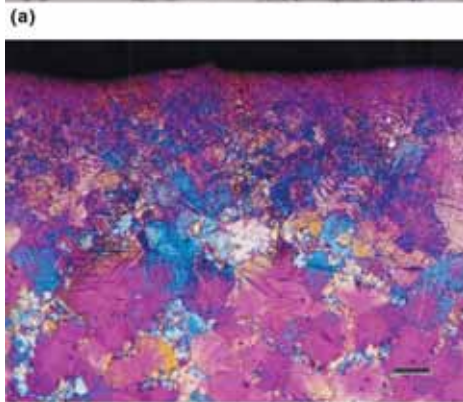
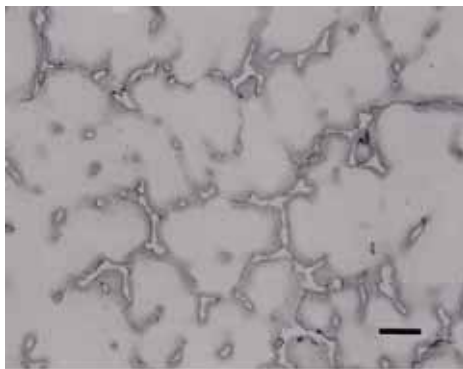


**Fig. 56** Microstructure of sand-cast AZ91C (Mg-9%Al-0.25%Mn-0.7%Zn-0.0008%Be) revealed (a) using acetic-glycol etch and viewed in bright-field illumination and (b) after etching with glycol and viewed with polarized light illumination plus a sensitive tint filter. Part (a) shows the general structure (primary  $\alpha$ -Mg grains, intergranular eutectic phase) after etching with acetic glycol. Part (b) is a lower-magnification view of the near-surface microstructure. Note the mechanical twins at the surface. (G.F. Vander Voort, Buehler Ltd.)

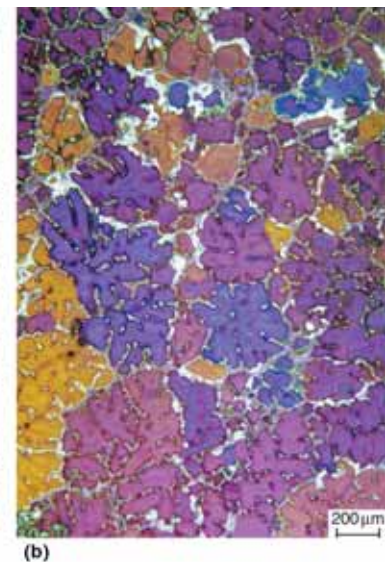
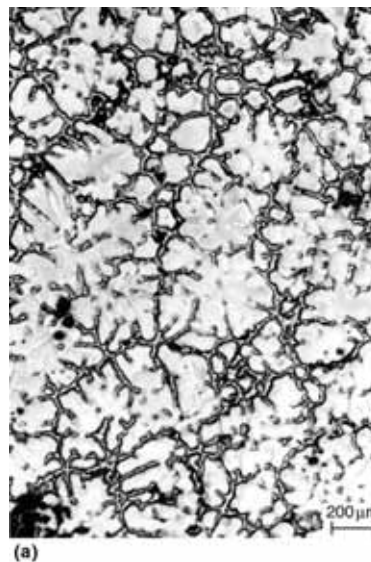


**Fig. 57** Comparison of (a) conventional etching and bright-field illumination with (b) electrolytic etching and polarized light illumination. Specimen is thixocast (semisolid process) AZ91. Electrolytic etching reveals individual grains by the coloration while retaining good contrast at the grain boundaries. The addition of color allows for identification of orientation of the grains, in addition to parameters such as shape factor, the ratio of minimum to maximum grain diameters, and so on. (E. Schaberger, Gießerei-Institut, RWTH Aachen)

# Metallography and Microstructures of Nickel and Nickel-Copper Alloys

William L. Mankins, Metallurgical Services, Inc.

THE PREPARATION of metallographic specimens and the microstructures of alloys containing 96% or more nickel (Nickel 200, Nickel 270, and Duranickel 301) and nickel-copper alloys (Monel 400, Monel R-405, and Monel K-500) are considered in this article. Micrographs of these alloys are shown in Fig. 1 to 15.

The procedures and materials for sectioning, mounting, grinding, and polishing specimens are essentially the same for all nickel alloys regardless of specimen size or sophistication of laboratory facilities. In preparing specimens for metallographic examination, it is important to prevent cold working of the surface during grinding/polishing steps.

## Preparation for Microscopic Examination

The specimen to be examined is cut to a convenient size with a silicon carbide water-cooled abrasive cutoff wheel, then mounted in a hard

plastic, such as Bakelite (Georgia-Pacific) or a hard epoxy resin. Next, the mounted specimen is ground flat on a belt grinder using 120-grit abrasive and water coolant. In general, it is preferable that the exposed area of the specimen not exceed approximately 1.6 cm<sup>2</sup> (0.25 in.<sup>2</sup>).

**Grinding** may be performed manually or on power-driven wheels using silicon carbide paper disks, starting with 220-grit and following with 320-, 400-, and 600-grit abrasives. The specimen is then washed thoroughly between grind steps and cleaned ultrasonically after final grinding to remove any abrasive particles remaining on the surface.

**Polishing.** All scratches from grinding are removed by polishing on a nylon cloth charged with 6 μm diamond paste and lubricated with lapping oil. An alternate method is to polish on a broadcloth-covered wheel using 5 μm levigated alumina (Al<sub>2</sub>O<sub>3</sub>) powder suspended in water.

Final polishing may be performed in one or two stages with a polishing wheel or vibratory polisher. If a polishing wheel is used, microcloth

and γ-Al<sub>2</sub>O<sub>3</sub> powder (<0.1 μm particle size) suspended in water are recommended. An alternative requires semifinal and final polishing using a vibratory polisher. Semifinal polishing employs a nylon polishing cloth and a slurry of 0.3 μm Al<sub>2</sub>O<sub>3</sub> and distilled water. A 350 g (12 oz) weight is placed on the specimen throughout the polishing cycle. At the conclusion of each polishing cycle, the specimen is cleaned ultrasonically. Final polishing employs a short-nap microcloth and a slurry of 0.05 μm Al<sub>2</sub>O<sub>3</sub> and distilled water. Polishing continues until the surface is free of scratches.

**Electropolishing.** Nickel and nickel-copper alloys can be electropolished satisfactorily, although best results are generally obtained with specimens that first have been polished mechanically through 600-grit abrasive. Recommended electrolytes and current densities for electropolishing these alloys are given in Table 1. A platinum cathode is suggested, and the electrolyte should be water cooled and continuously stirred.

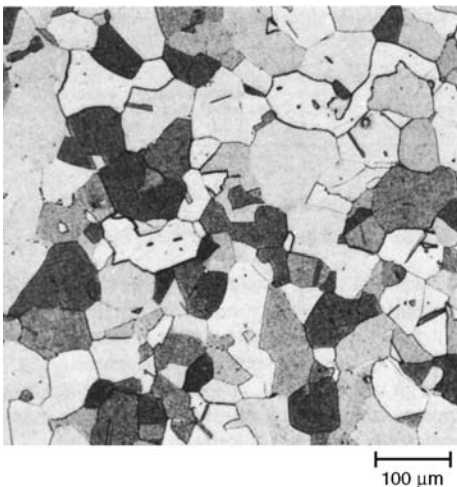


**Fig. 1** Nickel 200, cold drawn and annealed in a continuous process at 830 °C (1525 °F). Structure: nickel solid solution. See also Fig. 2. NaCN, (NH<sub>4</sub>)<sub>2</sub>S<sub>2</sub>O<sub>8</sub>. 100×

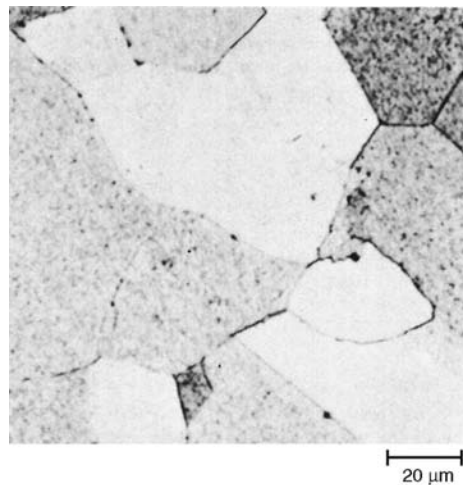


**Fig. 2** Same as Fig. 1 but at higher magnification. Variation in shade of grains is caused by variation in grain orientation. NaCN, (NH<sub>4</sub>)<sub>2</sub>S<sub>2</sub>O<sub>8</sub>. 500×

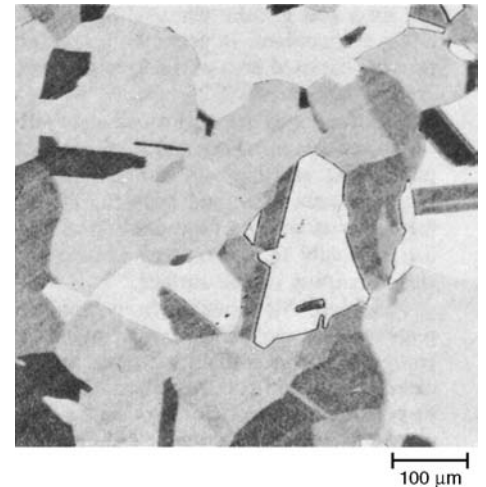


**Fig. 3** Nickel 270, hot rolled and annealed in a continuous process at 830 °C (1525 °F). Structure: nickel solid solution. See also Fig. 4. NaCN, (NH<sub>4</sub>)<sub>2</sub>S<sub>2</sub>O<sub>8</sub>. 100×

**Etching.** The solutions and conditions for etching nickel alloys for microscopic examination are described in Table 2. The acids used should be concentrated; when water is indicated, use distilled water only.

## Preparation for Macroscopic Examination

Surfaces to be etched for macroscopic examination may be prepared by surface grinding to a fine finish with 180-grit and 240-grit silicon carbide paper. Finer grinding, although unnecessary, yields a finer surface before etching, which requires less severe macroetching to reveal the metal structure.

Etching of nickel alloys for macroscopic examination is performed by immersing or swabbing the ground specimen for 5 to 20 s in an etchant composed of equal parts (by volume) of concentrated nitric acid ( $\text{HNO}_3$ ) and glacial acetic acid. Immersion etching may be preferred, because the metallographer can observe the surface being etched and terminate etching when features can be seen on the surface or a color change noted.

Macroetching of nickel-copper alloys is done by immersing or swabbing the ground specimen in concentrated  $\text{HNO}_3$ . Colorless acid should be used to avoid staining. Depending on the purpose of the examination, etching time should be 3 to 5 min. Within this range, shorter etching times will reveal sulfur embrittlement and details

of welds in Monel; longer times will reveal general structure, including surface and subsurface cracks, porosity, and forging flow lines. Ma-

**Table 1 Electrolytes and current densities for electropolishing of nickel and nickel-copper alloys**

Electrolyte composition	Applicable alloys	Current density	
		A/cm <sup>2</sup>	A/in. <sup>2</sup>
37 mL $\text{H}_3\text{PO}_4$ (conc), 56 mL glycerol, 7 mL $\text{H}_2\text{O}$	Nickel 200	1.4–1.5	9–10
	Nickel 270	1.5–1.8	10–12
	Duranickel 301	1.25–1.5	8–10
33 mL $\text{HNO}_3$ (conc), 66 mL methanol	Monel 400	0.9–1	6–7
	Monel 400, R-405, K-500	1.5–2.3	10–15

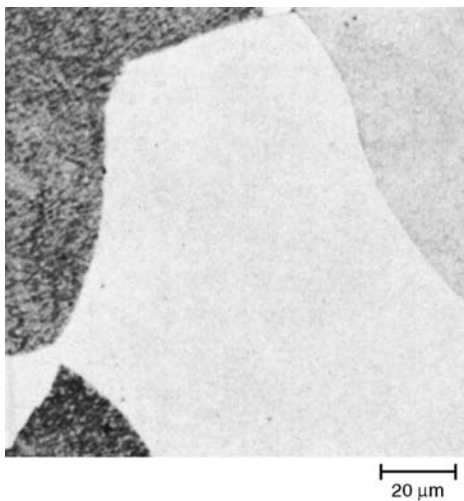


**Fig. 4** Same alloy and same processing as in Fig. 3 but shown at a higher magnification. The variation in shade of the grains (dark, gray, and white) is the result of variation in grain orientation. NaCN,  $(\text{NH}_4)_2\text{S}_2\text{O}_8$ . 500 $\times$

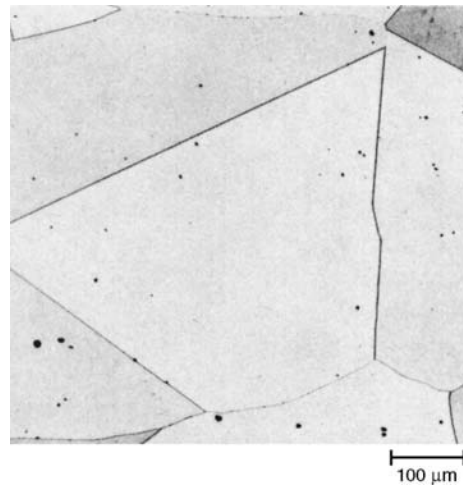


**Fig. 5** Permannickel 300, solution annealed 1 h at 1205 °C (2200 °F) and water quenched, aged 10 h at 480 °C (900 °F) and water quenched. Dispersed particles of TiN and graphite (black dots) in nickel solid solution. NaCN,  $(\text{NH}_4)_2\text{S}_2\text{O}_8$ . 100 $\times$

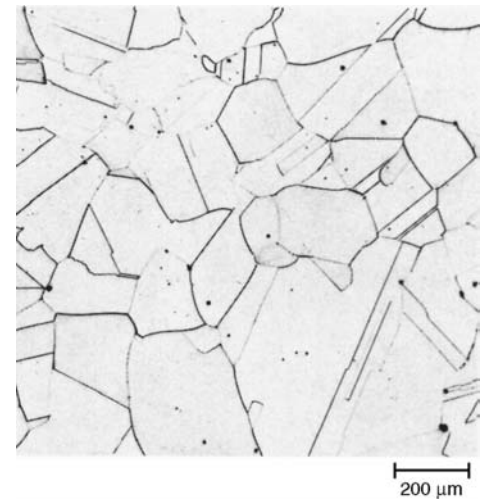


**Fig. 6** Duranickel 301, solution annealed for 30 min at 980 °C (1800 °F) and water quenched, aged for 20 h at 480 °C (900 °F) and water quenched. Microstructure: nickel solid solution; graphite particles (black dots). NaCN,  $(\text{NH}_4)_2\text{S}_2\text{O}_8$ . 50 $\times$

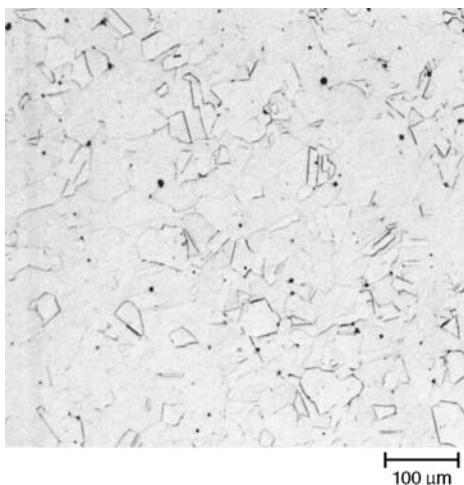


**Fig. 7** Monel 400, cold drawn and annealed in a continuous process at 830 °C (1525 °F). Nickel-copper solid solution with a few unidentified nonmetallic inclusions (black). NaCN,  $(\text{NH}_4)_2\text{S}_2\text{O}_8$ . 100 $\times$

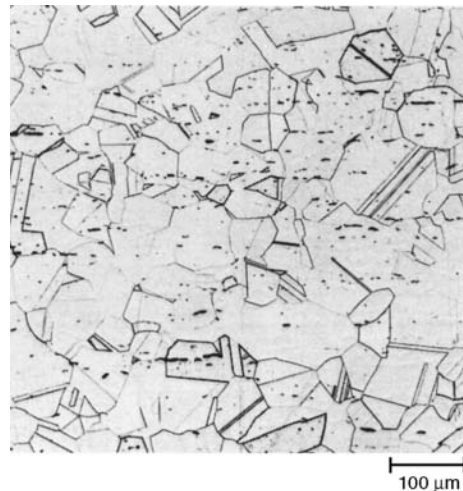


**Fig. 8** Monel R-405, cold drawn, and annealed in a continuous process at 830 °C (1525 °F). Microstructure: nickel-copper solid solution with sulfide stringers (black constituent). NaCN,  $(\text{NH}_4)_2\text{S}_2\text{O}_8$ . 100 $\times$

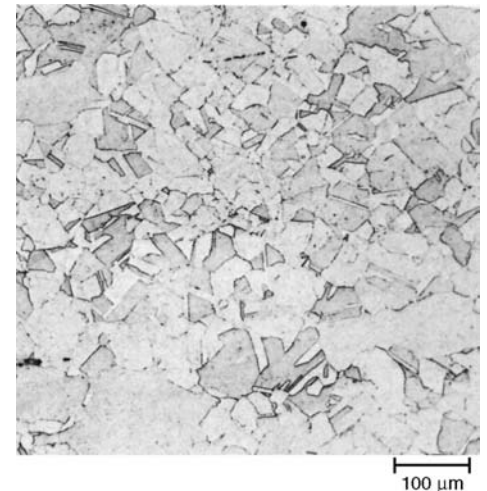


**Fig. 9** Monel K-500 in the hot rolled condition. Structure: nickel-copper solid solution. Variation in shade of grains is the result of variation in grain orientation. Glyceregia. 100 $\times$

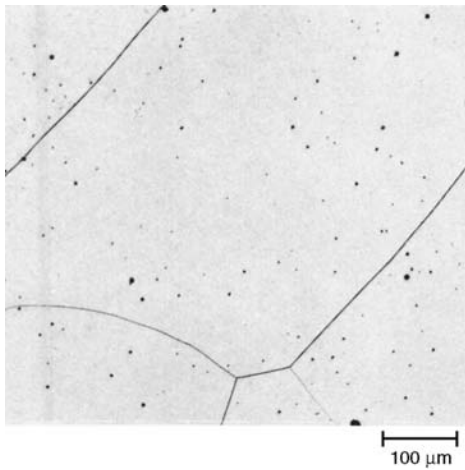


**Fig. 10** Monel K-500, solution annealed for 1 h at 1205 °C (2200 °F) and quenched in water. Nickel-copper solid-solution matrix. See also Fig. 11 to 15. NaCN, (NH<sub>4</sub>)<sub>2</sub>S<sub>2</sub>O<sub>8</sub>. 100×

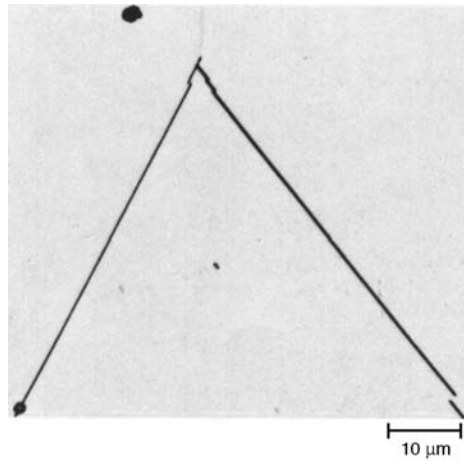


**Fig. 11** Same as Fig. 10 but at higher magnification. Portions of only three grains are visible. The black dots are nitride particles. See also Fig. 10 and 12 to 15. NaCN, (NH<sub>4</sub>)<sub>2</sub>S<sub>2</sub>O<sub>8</sub>. 1000×

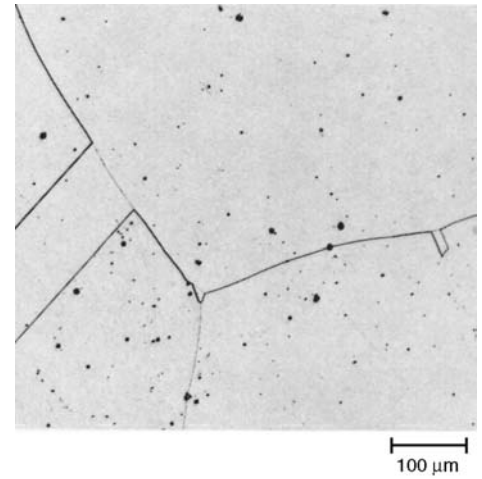


**Fig. 12** Monel K-500, held 1 h at 1205 °C (2200 °F), transferred to a furnace at 595 °C (1100 °F) and aged 4 h, water quenched. Solid-solution matrix; nitride particles. See also Fig. 10, 11, and 13 to 15. NaCN, (NH<sub>4</sub>)<sub>2</sub>S<sub>2</sub>O<sub>8</sub>. 100×

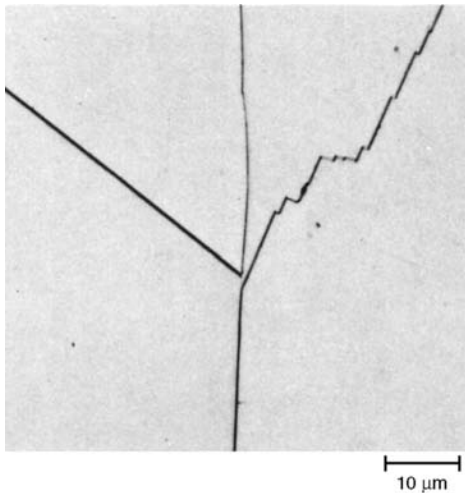


**Fig. 13** Same as Fig. 12 but at higher magnification. Structure contains precipitated Ni<sub>3</sub>(Al,Ti), resolvable only by electron microscopy unless aging temperature is higher than 595 °C (1100 °F). See also Fig. 10 to 12 and 14, 15. NaCN, (NH<sub>4</sub>)<sub>2</sub>S<sub>2</sub>O<sub>8</sub>. 1000×

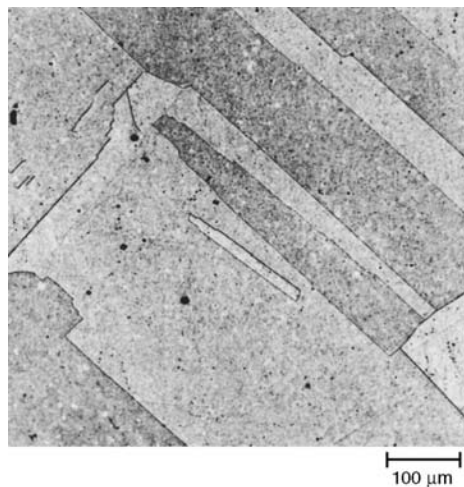


**Fig. 14** Monel K-500, held 1 h at 1205 °C (2200 °F), transferred to a furnace at 705 °C (1300 °F) and aged 4 h, water quenched. Precipitated Ni<sub>3</sub>(Al,Ti) appears as tiny particles dispersed in the matrix solid solution. See also Fig. 10 to 13 and 15. NaCN, (NH<sub>4</sub>)<sub>2</sub>S<sub>2</sub>O<sub>8</sub>. 100×

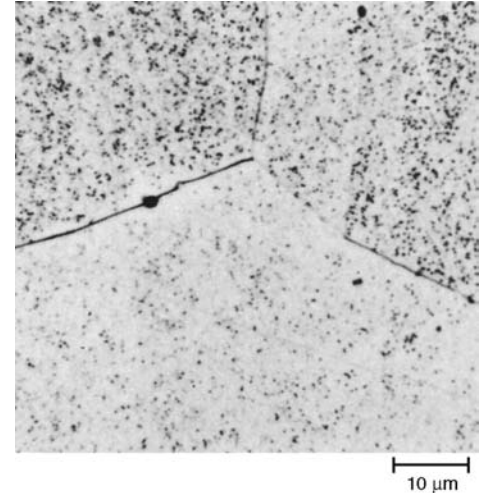


**Fig. 15** Same as Fig. 14 except at a higher magnification. The Ni<sub>3</sub>(Al,Ti) precipitate is better resolved. When this precipitate is resolvable by optical microscopy, overaging is indicated. See also Fig. 10 to 14. NaCN, (NH<sub>4</sub>)<sub>2</sub>S<sub>2</sub>O<sub>8</sub>. 1000×

**Table 2 Etchants for microscopic examination of nickel and nickel-copper alloys for grain boundaries and general structure**

Composition of etchant	Conditions for use
<b>Etchants for Nickel 200 and 270; Permanickel; Duranickel 301; and Monel 400, R-450, and K-500</b>	
1 part 10% aqueous solution of NaCN (sodium cyanide), 1 part 10% aqueous solution of (NH <sub>4</sub> ) <sub>2</sub> S <sub>2</sub> O <sub>8</sub> (ammonium persulfate). Mix solutions when ready to use.	Immerse or swab specimen for 5–90 s.(a)
1 part HNO <sub>3</sub> (conc), 1 part acetic acid (glacial). Use fresh solution.	For revealing grain boundaries. Immerse or swab specimen for 5–20 s.
7.5 mL HF, 2.5 mL HNO <sub>3</sub> , 200 mL methanol 5 g FeCl <sub>3</sub> , 50 mL HCl, 100 mL H <sub>2</sub> O	Immerse sample 2–4 min. Immerse or swab specimen up to a few minutes.
<b>Alternate etchant for Monel K-500</b>	
Glyceresia: 10 mL HNO <sub>3</sub> (conc), 20 mL HCl (conc), 30–40 mL glycerol	Etch by immersing or swabbing the specimen for 30 s to 5 min.
(a) This cyanide-containing etchant is very hazardous in its preparation and use. Cyanide, even in small quantities, as dust, solution, or fumes may be fatal when taken into the body. A fume hood must be used with this etchant.	

**Table 3 Nominal compositions of nickel and nickel-copper alloys**

Alloy	Composition
Nickel 200	99.5Ni-0.08C-0.18Mn-0.20Fe
Nickel 270	99.98Ni-0.01C
Permanickel 300	98.5Ni-0.20C-0.25Mn-0.30Fe-0.35Mg-0.40Ti
Duranickel 301	96.5Ni-0.15C-0.25Mn-0.30Fe-0.63Ti-4.38Al
Monel 400	66.5Ni-31.5Cu-0.15C-1.0Mn-1.25Fe
Monel R-405	66.5Ni-31.5Cu-0.15C-1.0Mn-1.25Fe-0.043S
Monel K-500	66.5Ni-29.5Cu-0.13C-0.75Mn-1.0Fe-0.60Ti-2.73Al

croetching can be hastened by warming the specimen in hot water prior to etching.

## Microstructures of Nickel and Nickel-Copper Alloys

Nickel-base alloys are widely used as high-temperature materials. Micrographs of such alloys are presented in the article "Metallography and Microstructures of Heat Resistant Alloys" in this Volume. The micrographs in this article show structures of nickel alloys that are used primarily for their resistance to corrosion and for other specialized applications. As shown in Table 3, these alloys range in nickel content from 66.5 to 99.98%.

The microstructure of Nickel 200 typically contains some nonmetallic inclusions (principally oxide). Prolonged exposure to temperatures from 425 to 650 °C (800 to 1200 °F) results in the precipitation of graphite from the nickel solid solution.

Although Nickel 270 (99.98% Ni) is less likely than Nickel 200 to contain nonmetallic inclusions, their structures are similar, assuming that mechanical working and thermal treatments are similar (compare Fig. 1 and 2 to Fig. 3 and 4). The very low carbon in Nickel 270 ( $\leq 0.01\%$ )

assumes the absence of graphite after long time exposures at elevated temperatures (425 to 650 °C, or 800 to 1200 °F).

Permanickel 300 is an age-hardening alloy that, in the solution-annealed condition, shows randomly dispersed particles of titanium nitride (TiN) and graphite when observed through an optical microscope. When subsequently age hardened, the alloy has a similar appearance (Fig. 5), but it also contains a fine granular precipitate. This phase is not resolvable by optical microscopy in material aged at a normal aging temperature (480 °C, or 900 °F) but is visible in overaged material. The phase or phases responsible for the age hardening of this alloy have not been positively identified. The mechanism appears to be a complex precipitate. It has been observed that in addition to nickel, carbon, magnesium, and titanium are required for full hardness. Precipitation of a compound such as  $\text{Ni}_3(\text{Mg,Ti})\text{C}_x$  seems likely during age hardening.

Duranickel 301, an age-hardening alloy, combines the corrosion resistance of unalloyed nickel with increased strength and hardness. After solution annealing, this alloy is age hardened by holding in the temperature range of 425 to 705 °C (800 to 1300 °F), which precipitates the phase  $\text{Ni}_3(\text{Al,Ti})$  throughout the structure. In the

solution-annealed and properly aged condition (Fig. 6), the precipitated phase is not resolved by an optical microscope, but hardness effects are easily measured. Some particles of graphite, however, are usually visible.

**Nickel-Copper Alloys.** Monel 400 is a widely used stable solid-solution alloy of nickel and copper. Nonmetallic inclusions often appear in the microstructure (Fig. 7).

Monel R-405 is a free-machining grade of Monel 400 produced with an intentional addition of sulfur (0.025 to 0.050%). The microstructures of these two alloys are similar for the same hot/cold working history of mechanical and thermal treatment, except for the sulfide particles in Monel R-405, which improve its machinability (Fig. 8).

Monel K-500 is produced by adding aluminum and titanium to the basic nickel-copper composition. Solution annealing and aging produce a  $\gamma'$  precipitate throughout the matrix. In material aged at the normal temperature of 595 °C (1100 °F), this precipitate is not resolvable by an optical microscope (Fig. 12, 13). However, in material that is overaged—by holding at 705 °C (1300 °F), for example—the precipitate is visible by optical microscopy (Fig. 14, 15). In addition to the precipitate, particles of TiN are usually present in the microstructure.

# Metallography and Microstructures of Precious Metals and Precious Metal Alloys

Elma van der Lingen, Lesley Cornish, Stefanie Taylor, Rainer Süß, Physical Metallurgy Division, Mintek, South Africa; Stewart Grice, Hoover & Strong Inc.

THE PRECIOUS METALS include the six platinum-group metals (platinum, palladium, rhodium, ruthenium, iridium, and osmium) as well as gold and silver. These elements share properties such as inert softness, crystal structure, relatively high density, and good corrosion resistance, which directly influence their metallographic preparation. The crystal structure of both ruthenium and osmium is hexagonal close-packed (hcp), whereas the other precious metals have a face-centered cubic (fcc) structure. The hcp structure of ruthenium and osmium makes it possible to use polarized light for metallographic investigations. The fcc structure is generally relatively soft, and Vickers hardness values are under 50 for fine platinum, palladium, gold, and silver in the annealed condition. All the precious metals are relatively dense, with values varying between 10.5 g/cm<sup>3</sup> (0.379 lb/in.<sup>3</sup>) for silver to 22.65 g/cm<sup>3</sup> (0.818 lb/in.<sup>3</sup>) for iridium.

Precious metals are known primarily for their use in money and jewelry. However, they also have industrial applications, including catalysis, high-temperature applications, electrical contacts, electronics, corrosion resistance, and dental and medical uses.

## Specimen Preparation

Due to the high cost of material, precious metals samples for metallographic investigations are usually small, which makes mounting of specimens exacting. The following steps are generally followed for preparing good metallographic samples (Ref 1, 2).

**Cutting.** Precious metals should be cut with sharp cutting tools. When cutting wheels are used, adequate coolant is required to prevent structural changes and smearing (Ref 1).

**Mounting.** Thermosetting epoxy resin is the main medium employed for mounting of precious metals. Precious metals are often used as

coatings. To prevent damage to the coating during polishing, plating of specimens before mounting is recommended. Copper, nickel, or rhodium are most often used for plating (Ref 3). Lubricants for mount releasing should be omitted, because fine cracks form between the specimen and the mount, resulting in subsequent polishing and etching problems (Ref 2).

**Grinding.** Coarse grinding on 80- and 120-grit SiC paper is recommended to remove the deformation layer formed during sectioning. A specimen that has not been subjected to cutting can be ground on a succession of 240- to 2400-grit SiC paper. Moderate pressure is employed, with running water as a lubricant. Samples can be rinsed, but a short cycle of ultrasonic cleaning is recommended to remove any impurities after each paper. Ultrasonic cleaning should be limited to less than 30 s to avoid cavitation (Ref 2).

**Polishing.** Coarse polishing should be done with a napless cotton cloth with 6 µm polycrystalline diamond, odorless kerosene, or diamond extender lubricant and moderate pressure.

Fine polishing should be carried out using a short-napped synthetic velvet cloth with 1 µm polycrystalline diamond and deionized water lubricant, using moderate to light pressure. After polishing, the sample can be cleaned ultrasonically in detergent and rinsed with methanol to aid water evaporation and to minimize watermarks on the polished microsections, then air dried.

Because of the hardness range of precious metals, the polishing time varies from material to material. Microscopic investigation between polishing steps is recommended to determine when scratches from the previous step have been removed and to avoid overpolishing (Ref 2).

**Etchants.** The four etching techniques that are often used for precious metals include immersion, swab, etch polishing, and electrolytic etching. Due to the extreme corrosion resistance of precious metals, the etchants used are very cor-

rosive and can be hazardous. In many cases, etchants need to be heated, which further increases the risks. The hazards of working with the relevant chemicals should be well understood, and appropriate safety precautions should be followed. For example, all etching should be conducted under a properly operating chemical fume hood, and inhalation of fumes from etchants should be avoided. Appropriate safety equipment, such as an acid-protective apron, gloves, and face shield or goggles, should be used. Disposal of the spent etchant must be in accordance with local legal requirements (Ref 2).

A list of etchants for precious metals and their alloys is given in Table 1 (Ref 1, 2, 4).

## Microstructures of Gold and Gold Alloys

### Pure Gold

Figures 117–119, in the article “Selected Color Images” in this Volume show macrostructures of a sectioned 1kg 99.99% pure gold bar. The grain morphology in the gold bars varies due to the different cooling mechanisms after casting. The samples were etched in boiling aqua regia (HCl to HNO<sub>3</sub>: 3 to 1) for 10 to 20 s. Several polishing/etching cycles were done to obtain a scratch-free and stress-free surface. A significant difference can be seen between two smaller cast gold bars, one of which shows equiaxed grains (Fig. 120 in the article “Selected Color Images”), while a cold stamped bar reveals a very fine, disordered grain structure in a stamped bar (Fig. 121).

### Gold Jewelry Alloys

Pure gold is very soft and is considered the most malleable of all metals. Jewelry items are